HYDRATION TEMPERATURE RISE AND THERMAL STRESSES INDUCED IN SEGMENT-ON-PIER OF PRESTRESSED CONCRETE BOX GIRDER BRIDGE

P.L. Ng [1,*], J.S. Du [2], X.F. Luo [2] and F.T.K. Au [1]
[1] Department of Civil Engineering, The University of Hong Kong, Pokfulam, Hong Kong, China
[2] School of Civil Engineering, Beijing Jiaotong University, Beijing, 100044, China
*Email: irdngpl@gmail.com.

ABSTRACT

The heat generation from chemical reactions of hardening concrete causes temperature rise and thermal expansion. When the concrete temperature eventually cools down to the ambient, thermal contraction would result. If the tendency of volume change and associated thermal movement are restrained, thermal stresses would be induced and this would lead to early thermal cracking. The issue of thermal cracking should be duly considered in mass concrete construction. Regarding concrete bridge construction, the piles, pile caps, bridge piers, crosshead girders, and bridge diaphragms are typical examples of mass concrete elements. A bridge project in real-life is selected for study in this paper, with focus on the segment-on-pier accommodating the diaphragm of prestressed concrete girder deck. The segment was instrumented to measure its actual early age temperature rise on site. Finite element simulation and analysis was conducted to evaluate the time variations of temperature distributions and thermal stresses induced in the bridge segment. The risk of thermal cracking can be indicated by the measurement and analysis results. The techniques employed in this study are useful for planning of temperature control measures in similar projects.

KEYWORDS

Bridge segment, finite element method, heat generation, temperature rise, thermal stress.

INTRODUCTION

When concrete is under curing and hardening, the exothermic chemical reactions of cementitious materials liberate heat and cause the temperature of concrete to rise at its early age. Due to variable distances within the concrete members to the boundary and variable boundary conditions, the temperature rise is in general non-uniform. Near to the surfaces, the temperature is closer to the ambient temperature, while within the interior of the concrete member, the temperature is higher. The non-uniformity of temperature distribution within mass concrete structures is particularly apparent (ACI Committee 207 2005). Subsequently, when the temperature of the concrete eventually drops to the ambient, the concrete tends to contract. If the tendency of volume change and the associated thermal movement are restrained, tensile stresses are induced in the concrete, and early age thermal cracking would result if the restrained tensile strain exceeds the tensile strain capacity of concrete.

The occurrence of thermal cracking would impair the structural integrity, serviceability, durability and appearance of concrete structures. Hence, it is imperative to prevent or mitigate the thermal cracking problem. Such necessitates the control of both the maximum temperature and temperature differential of concrete structures (Bamforth 2007). Depending on the characteristics of the project and the movement constraints, different measures such as pre-cooling of ingredients before concrete batching/placing, installing internal cooling pipes, mist spraying, optimizing concrete mix design, insulating/cooling the formwork and optimizing formwork striking time may be applied (Kwan et al. 2004; Bamforth 2007). Theoretically speaking, the choice of measures or combinations of measures should be based on proper modelling and analysis of the thermal regime of structures and its time-variation (Springenschmid 1995). These are usually performed by means of finite element method (De Schutter 2002; Du et al. 2011).

The mitigation of thermal cracking and design of temperature control measures for massive concrete structures should be duly considered. In the construction of concrete bridges, the piles, pile caps, bridge piers, crosshead girders and diaphragms are examples of massive concrete members to which special attention on thermal cracking control should be paid. Based on a prestressed concrete box girder bridge project in real life, this paper reports the on-site monitoring of early age temperature rise and finite element analysis of temperature distributions and thermal stresses induced in a segment-on-pier accommodating the diaphragm of prestressed concrete girder deck. Details of the bridge and the segment-on-pier under investigation will be presented in the following sections.

BACKGROUND INFORMATION OF BRIDGE AND SEGMENT-ON-PIER

Structural Form of Bridge

The bridge chosen for study is Jinghe Bridge in Mainland China. Jinghe Bridge is located in Qingyang, Gansu Province. It forms part of the Zhangfeng Expressway in northwest China. The total length of bridge is 1,726 m and the main spans are arranged in lengths of (87 + 162×5 + 87) m, as shown in Figure 1. The bridge deck is haunched over each span for improved structural efficiency and aesthetics. Construction started in 2009. The bridge piers and the segment-on-pier for the main spans were cast in-situ components, upon which continuous prestressed concrete box girder decks with variable depth were constructed by balanced cantilever method (Du et al. 2011).

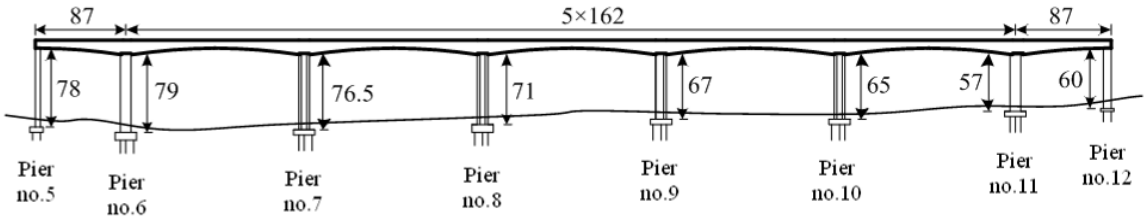

Figure 1 Main spans of Jinghe Bridge (dimensions in m)

Structure and Materials of Segment-on-Pier

The segments-on-pier over bridge piers nos. 7 to 10 are selected for study. The 4 nos. segments-on-pier have common geometry as depicted in the typical cross section and elevation in Figure 2. Each segment has a transverse width of 6.5 m at the pier head and 12.0 m at the top flange. The structural height of segment is 9.5 m and the length in longitudinal direction is 9.0 m, along which the segment is provided with three cellular voids. The voids are separated by 0.5 m thick solid diaphragms each with a horseshoe shaped opening of 1.2 m in width and 2.0 m in height at the centre. The cellular voids are of 4.9 m width in transverse direction and 7.75 m in height. The middle cellular void directly above the axis of bridge pier has length of 3.0 m in the longitudinal direction and the cellular voids at its two sides both have length of 2.0 m.

The bottom flange of the segment-on-pier has thickness of 1.3 m. The webs are vertical and have thickness of 0.8 m. The top flange is tapered with gradual reduction in thickness away from the root of webs. Its thickness at the centreline of the girder section is 0.45 m. The surface level of top flange follows a transverse gradient of 2%. To reduce stress concentrations, chamfers and splays are provided at corners and at changes in sections.

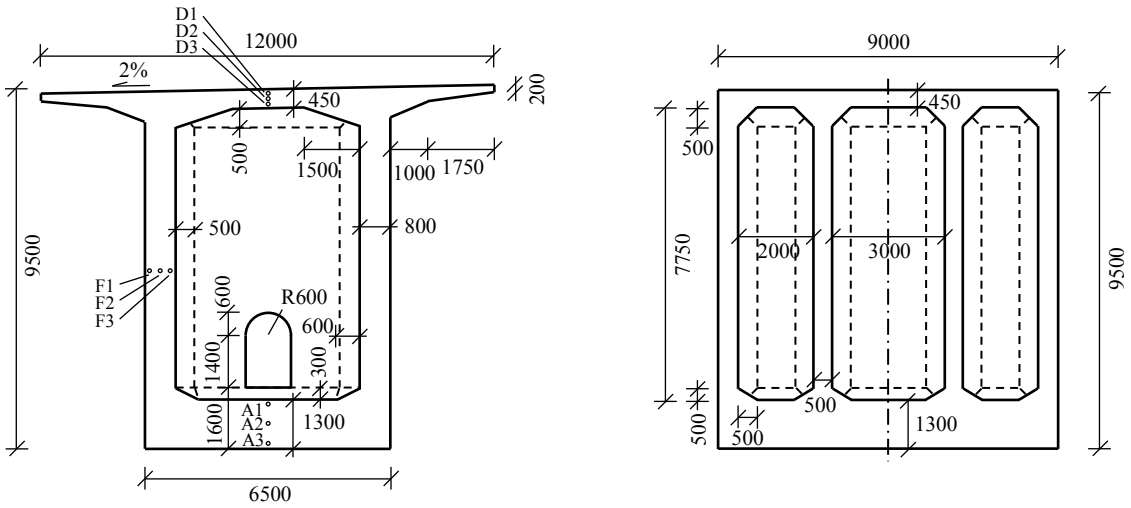

(a) Typical cross section (b) Typical elevation

Figure 2 Geometry of segment-on-pier (dimensions in mm)

The segment-on-pier was cast of C55 concrete. Three mix proportions as tabulated in Table 1 had been proposed and they are hereunder designated as Mix 1, Mix 2 and Mix 3. Mix 1 is a cement concrete mix, Mixes 2 and 3 contain pulverized fuel ash (PFA) in the binder at a replacement rate of approximately 17% by mass, with the aim to reduce the cement content and hence the heat of hydration (Ng et al., 2011; Ng and Kwan 2012). The water to binder (W/B) ratio by mass of Mixes 1, 2 and 3 are 0.33, 0.25 and 0.26 respectively, and the paste volume of all three mixes is about 27%. Plywood of 20 mm thickness was adopted for external formwork for concrete casting, while 3 mm thick prefabricated steel formwork was used internally. The convection heat transfer coefficients of the wooden and steel formwork were evaluated to be 3.98 and 17.26 $W/m^2/^oC$ respectively.

Table 1 Concrete mix proportions

	Mix 1	Mix 2	Mix 3
Water content (kg/m^3)	163	135	133
Cement content (kg/m^3)	494	451	423
PFA content (kg/m^3)	0	92	86
Fine aggregate (kg/m^3)	681	663	711
Coarse aggregate (kg/m^3)	1112	1118	1100
Admixture (kg/m^3)	5.93	5.97	5.60

MEASUREMENT OF HYDRATION TEMPERATURE RISE

To measure the temperature rise of the segment-on-pier after casting, temperature sensors were embedded at the segment cross-section intersecting the centre of pier. A total of 9 sensors were employed, with 3 sensors at middle of top flange, mid-height of one web, and middle of bottom flange, respectively. The sensors were Type RT resistance temperature detectors designed for embedment in concrete structures. The measurement range, resolution and accuracy of the sensors were -40ºC to 150ºC, ±0.1ºC and ±0.3ºC, respectively. The numbering of sensors is shown in Figure 2(a). At the top flange, 3 sensors, designated as D1, D2 and D3 were embedded along the centreline of section near the upper surface, middle of thickness, and near the lower surface, respectively. At the web, 3 sensors, designated as F1, F2 and F3 were embedded at the mid-height of segment near the external surface, middle of thickness, and near the internal surface, respectively. At the bottom flange, 3 sensors, designated as A1, A2 and A3 were embedded along the centreline of section near the upper surface, middle of thickness, and near the lower surface, respectively. The measurement of temperature enabled comparison with established acceptable limits of peak temperature and thermal gradient, which are usually taken as 70ºC (MTRC 2009) and 20ºC/m (MTRC 2009; Architectural Services Department 2011), respectively.

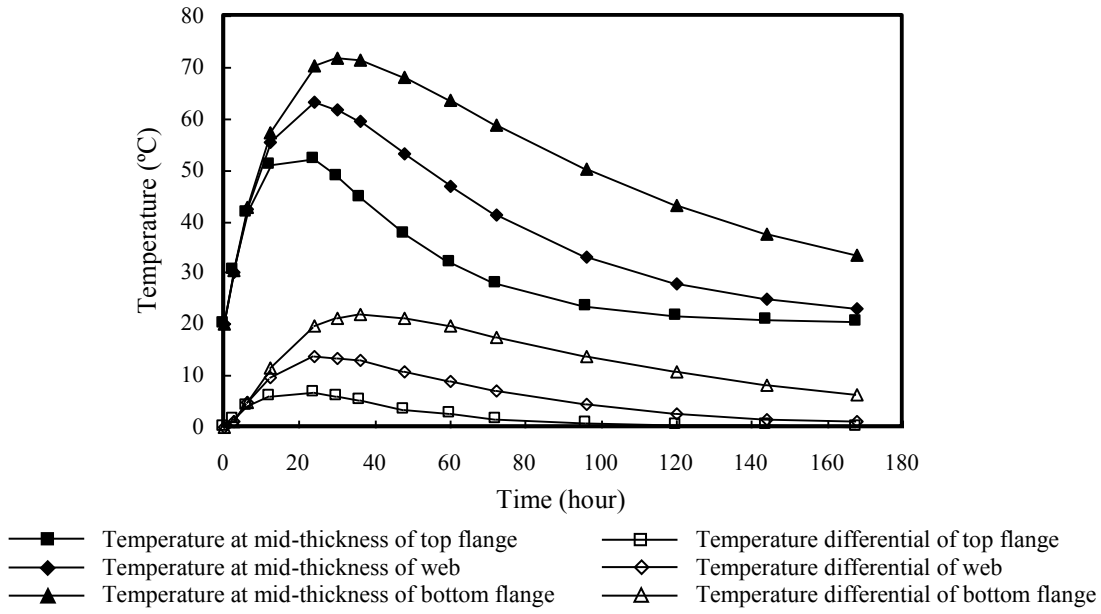

Figure 3 Variation of measured temperature with time

The temperature rise of the bridge pier was monitored continuously over the first 7 days after casting. The ambient temperature was also measured. Throughout the casting and curing of segment, the ambient temperature varied between 15ºC and 25ºC with a mean temperature of 20ºC. Figure 3 displays the variation of measured temperature with time. It can be seen that the peak temperature of concrete was reached generally at 24 to 30 hours after casting. The maximum temperatures of the top flange, web, and bottom flange were 52.3ºC (attained at 24 hours after casting), 63.3ºC (attained at 25 hours after casting), and 71.7 ºC (attained at 30 hours after casting), respectively. Though the first two values were smaller than the 70ºC limit, the last value was larger than the 70ºC limit and might be incurring excessive thermal movement (Bamforth 2007). The maximum temperature differentials across the mid-thickness and near-surface sensors at the top flange, web, and bottom flange were respectively 6.6ºC (attained at 25 hours after casting), 13.7ºC (attained at 26 hours after casting), and 21.9ºC (attained at 36 hours after casting). It is noted that the time to attain the maximum temperature differentials is generally longer than the time to attain the peak temperature. Dividing the temperature differentials by half the concrete thicknesses, the corresponding thermal gradients are 29.3ºC/m, 34.3ºC/m and 33.7ºC/m, which are all larger than the 20ºC/m limit and might cause excessive differential thermal stresses (Bamforth 2007). Therefore, the vulnerability of the segments-on-pier to thermal cracking should be studied in detail and duly mitigated.

FINITE ELEMENT ANALYSIS OF TEMPERATURE EFFECTS

Numerical analysis was conducted by finite element method to compute the temperature and stress distributions using the commercial software Midas-FEA. By virtue of symmetry, one quarter of the segment-on-pier was modelled by 6,572 four-node tetrahedron finite elements. In the following discussions, *x*-direction is the longitudinal direction along the span of bridge deck, *y*-direction is the transverse direction and *z*-direction is the vertical direction. Figure 4 depicts the finite element model. The tension-positive sign convention is adopted. The properties of concrete elements used in analysis are presented in Table 2.

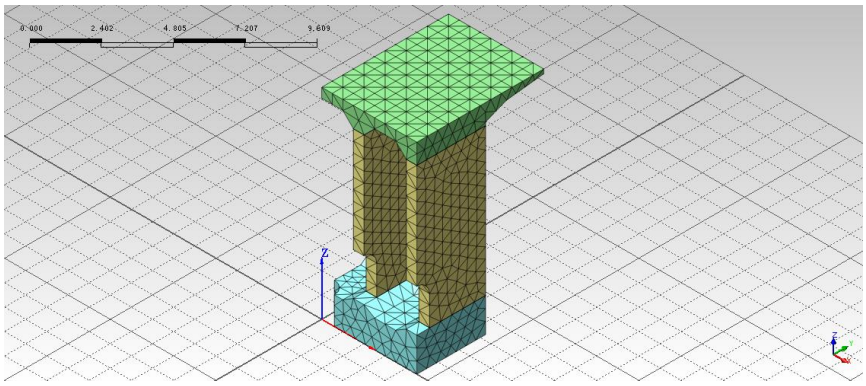

Figure 4 Finite element model of segment-on-pier

Table 2 Properties of concrete elements

Elastic modulus at age of 28 days (GPa)	35.5
Poisson's ratio	0.2
Tensile strength at age of 28 days (MPa)	2.74
Coefficient of thermal expansion (με/ºC)	10
Specific heat capacity (J/kg/ºC)	954
Thermal conductivity (W/m/ºC)	2.92
Convection heat transfer coefficient ($W/m^2/ºC$)	18.72
Density (kg/m^3)	2460

Computation of Temperature Distribution

The analysis took into account the actual construction sequence. The ambient temperature was assumed to be constant at 20ºC. Since the segment-on-pier is situated on the bridge pier, the presence of the bridge pier was simulated in the boundary conditions. To model the temperature rise during concrete hardening, step-by-step integration in the time domain was performed with the heat generation of concrete described by the time-varying function $H(t)$, which is given in the following equation proposed by Zhu (1998):

$$H(t) = H_o \cdot \left[1 - \exp\left(-at^b\right)\right] \quad (1)$$

where H_o is the ultimate heat generation of concrete evaluated as 145.4 MJ/m^3, a and b are coefficients dependent on the concrete properties and are taken respectively as 0.69 and 0.56, and t is the age expressed in days. The term inside the square bracket on the right hand side of Equation (1) is the maturity function of concrete. The adiabatic temperature rise of concrete at age t, $T_A(t)$, is estimated by Zhu (1998):

$$T_A(t) = \frac{H(t) \cdot (C + k_e P)}{\psi \rho} \quad (2)$$

where C (kg/m^3) is the cement content, P (kg/m^3) is the PFA content, k_e is the cement equivalence factor of PFA, ψ (J/kg/ºC) is the specific heat capacity of concrete, and ρ (kg/m^3) is the density of concrete. When the heat generation of concrete is at its ultimate, the adiabatic temperature rise was computed as 65.9ºC.

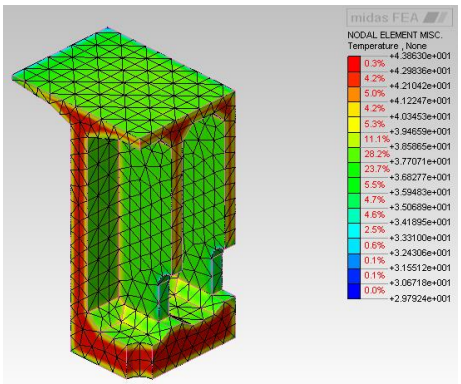

(a) 6 hours after concrete casting

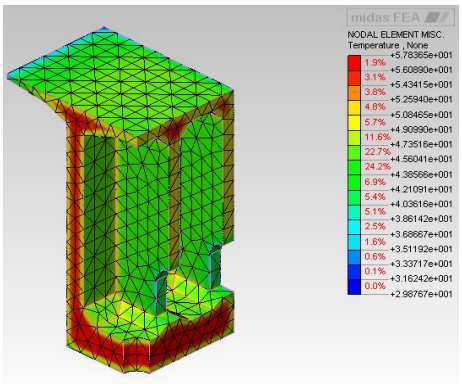

(b) 12 hours after concrete casting

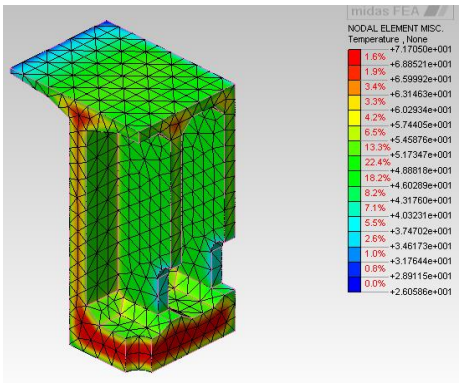

(c) 24 hours after concrete casting

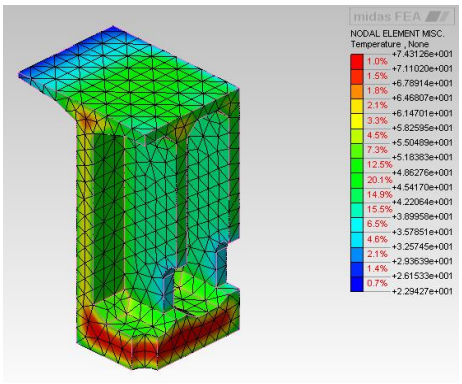

(d) 36 hours after concrete casting

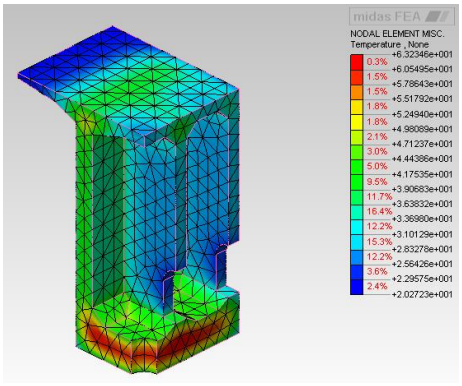

(e) 72 hours after concrete casting

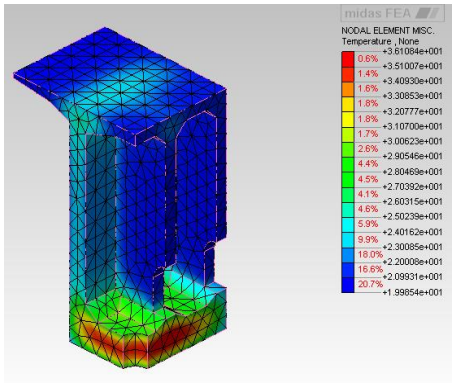

(f) 168 hours after concrete casting

Figure 5 Computed temperature distributions

The temperature distributions within the segment-on-pier at different time after concrete casting were determined from finite element analysis and are depicted in Figure 5. It is observed that the difference between the measured and computed temperature values is generally less than 2ºC, demonstrating the reliability of the finite element analysis. Nonetheless, measures such as increasing the fineness of the finite element mesh are advisable to further improve the accuracy of analysis.

Evaluation of Thermal Stresses and Cracking

During hardening, the elastic modulus of concrete increases, as described by Equation (3) in accordance with CEB-FIP Model Code 1990 (Comite Euro-International du Beton 1993):

$$E_c(t) = E_{co} \cdot \exp\left[0.5s\left(1 - \sqrt{28/t}\right)\right] \quad (3)$$

where E_{co} is the elastic modulus of concrete at age of 28 days, s is a coefficient depending on the type of cement (taken as 0.25 for ordinary Portland cement), and t is expressed in days.

The stresses in all elements at each time step were computed. Figure 6 plots the element stresses in x-, y- and z-directions at the instrumented locations. It is evident that during concrete curing, generally higher tensile stresses would develop near the external and internal concrete surfaces, whereas concrete around mid-thickness would remain compressive or subject to a small tensile stress. The thermal stresses induced in the bottom flange are having larger magnitudes than those in the top flange and web. This indicates that the magnitude of thermal stresses increases with the thickness of concrete. The analysis results revealed that the peak tensile stresses occurred approximately at the same time when the temperature differential across the concrete thickness was the largest. The computed maximum tensile stress was 1.71 MPa, occurring at the upper surface of the bottom flange at 36 hours after casting. When the concrete was cooling down in subsequence, stresses of the opposite signs would gradually develop.

To assess the vulnerability of the segment-on-pier to thermal cracking, the computed tensile stresses are checked against the tensile strength of concrete. The concrete tensile strength at different time is evaluated per Equation (4) in accordance with Model Code 1990 (Comite Euro-International du Beton 1993):

$$f_t(t) = f_{to} \cdot \exp\left[s\left(1 - \sqrt{28/t}\right)\right] \quad (4)$$

where f_{to} is the tensile strength of concrete at age of 28 days. The development of tensile strength of concrete with time is juxtaposed in Figure 6. It is seen that the computed tensile stresses in both x- and y-directions are higher than the tensile strength over certain time intervals, especially during the first 2 days after concrete casting. Therefore, the tensile strain capacity of concrete would possibly be exceeded and the segment-on-pier might exhibit cracking if additional temperature control measures are not provided.

EFFECTIVENESS OF THERMAL CRACKING CONTROL MEASURES

Use of PFA Concrete Mixes

To examine the effect on using PFA concrete mixes, finite element analyses were conducted for the scenarios of adopting Mixes 1, 2 and 3 for casting the segment-on-pier for comparison. Based on Equation (2), it is estimated that the adiabatic temperature rise of these 3 mixes are respectively 65.9ºC, 61.6ºC and 58.5ºC. The computed peak temperature, maximum temperature differential, and maximum tensile stress with respect to each of the 3 concrete mixes are tabulated in Table 3.

From Table 3, it is evident that by incorporation of PFA in the concrete mix to reduce the cement content, all the peak temperature, maximum temperature differential, and maximum tensile stress are reduced. Amongst the 3 concrete mixes, Mix 3 which has the lowest cement content is the most effective. The associated reductions in the peak temperature, maximum temperature differential, and maximum tensile stress are greatest at the bottom flange and are respectively 6.13ºC, 3.41ºC, and 0.18 MPa. It should be noted that though the maximum temperature is reduced to less than 70ºC, the thermal gradient is still as high as 28.4ºC/m and the tensile stress is still exceeding the tensile strength of concrete at the corresponding early age. Therefore, further optimisation of the concrete mix to lower the heat generation such as by incorporation of ground granulated blastfurnace slag and limestone fines and/or combining with other thermal cracking control measures are recommended.

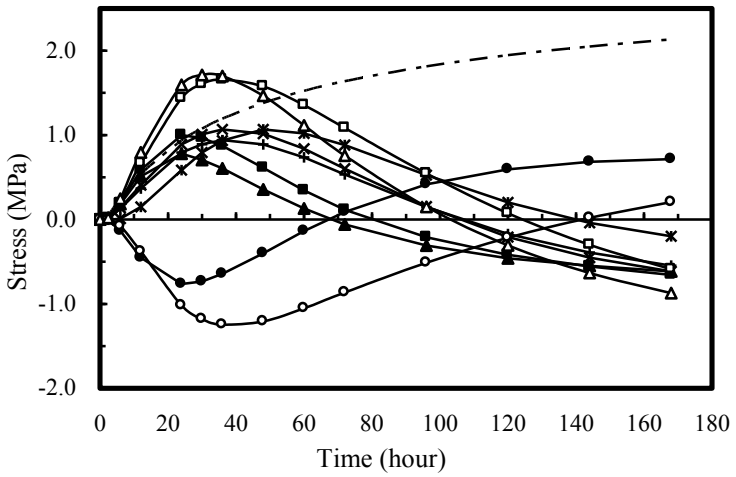

(a) Variations of stresses in *x*-direction

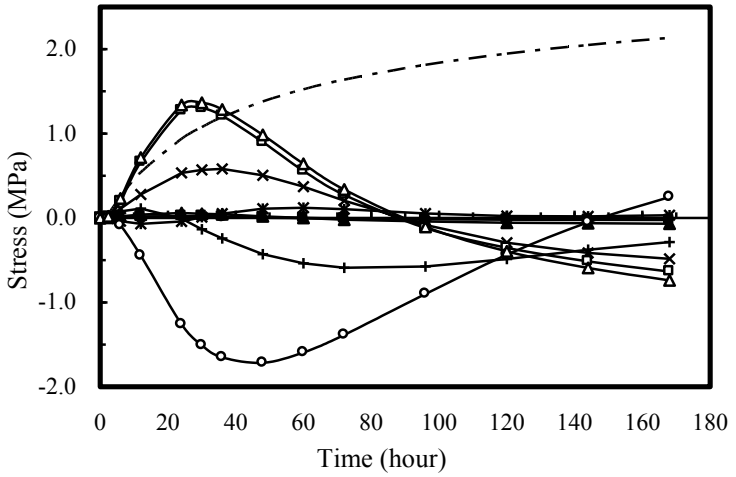

(b) Variations of stresses in *y*-direction

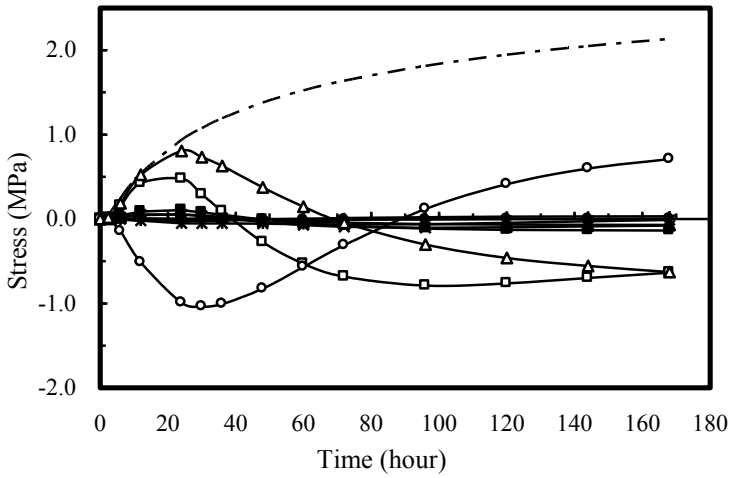

(c) Variations of stresses in *z*-direction

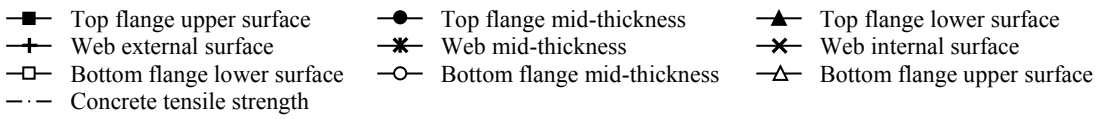

Figure 6 Variations of stresses with time

Table 3 Effects of different concrete mixes

	Mix 1			Mix 2			Mix 3		
Location	Top flange	Web	Bottom flange	Top flange	Web	Bottom flange	Top flange	Web	Bottom flange
Peak temperature (ºC)	52.27	63.25	71.67	50.17	61.86	68.83	48.52	58.75	65.54
Max. temperature differential (ºC)	6.58	13.72	21.90	5.72	12.03	19.32	4.81	11.12	18.49
Max. tensile stress (MPa)	1.07	1.00	1.71	0.99	0.97	1.59	0.98	0.94	1.53

Concrete Casting in Lifts

In view of the congested arrangement of prestressed tendon ducts and reinforcing bars inside the segment (this also precludes the embedment of internal cooling pipes), as well as the large quantity of concrete placement and difficulties in concreting, casting of the segment-on-pier in separate lifts was considered from constructability and from quality control viewpoints. Alternative casting schedules were simulated by finite element analyses before putting into practice. The segment with total height of 9.5 m is divided into 2 lifts, the first lift being 4.5 m in height and the second lift being 5.0 m in height. The time interval between the first and second concrete casting is 6 days.

By adopting casting in lifts, the computed time variations of temperature at mid-thickness of top flange, web and bottom flange are plotted in Figure 7. In the same figure, the computed temperature differentials at the top flange, web and bottom flange are plotted. Temperature distributions within the cast segment portion at different time were obtained from step-by-step time integration of the finite element analysis. The temperature distribution within the partially completed segment-on-pier at 24 hours after casting the first lift and the temperature distribution within the completed segment-on-pier at 24 hours after casting the second lift as determined from the analysis are depicted in Figure 8.

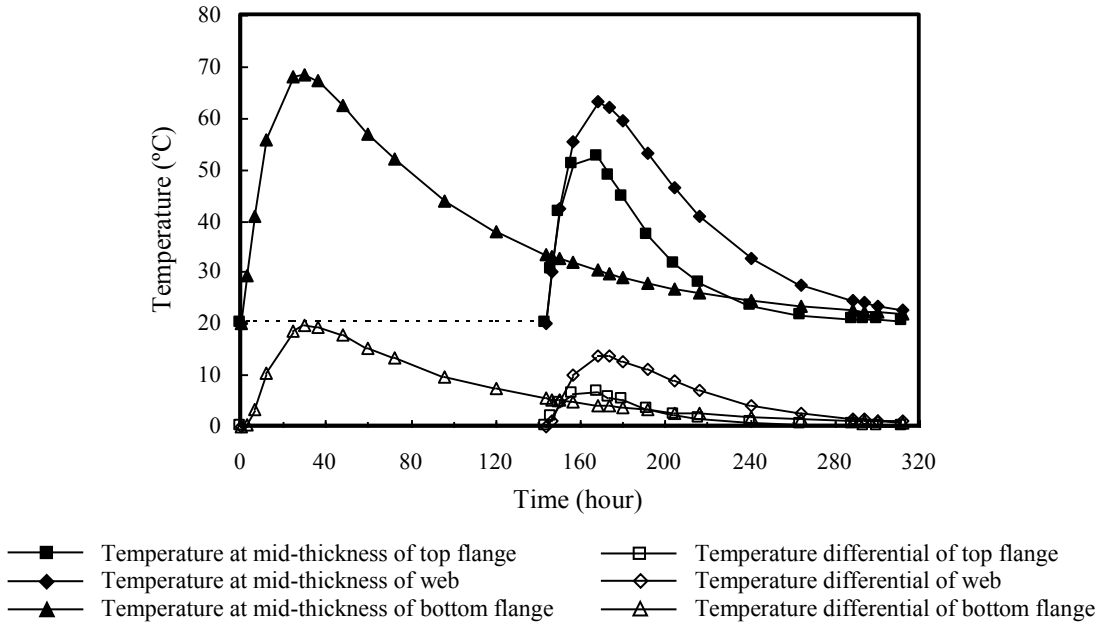

Figure 7 Time variation of temperature with casting in lifts

From the analysis results, the peak temperatures at the mid-thickness of top flange, web and bottom flange are respectively 52.3ºC, 63.3ºC and 68.6ºC, and the maximum temperature differentials at top flange, web and bottom flange are respectively 6.6ºC, 13.7ºC and 19.6ºC. The computed peak temperature, maximum temperature differential, and maximum tensile stress with respect to each casting schedule are tabulated in Table 4. It can be seen that casting in 2 lifts does not have significant effect in mitigating the temperature rises and

thermal stresses at the top flange and web. Nevertheless, the mitigation effect is more significant at the bottom flange. The peak temperature at mid-thickness of bottom flange is decreased by 3.03ºC, and the maximum temperature differential at bottom flange is decreased by 2.31ºC. This is mainly due to the increased exposed surface area of the bottom flange (in the absence of upper portion of the segment-on-pier) for more effective heat dissipation. On the other hand, the boundary conditions of the upper portion of segment after being cast are not significantly altered. With the reduction in maximum temperature differential at the bottom flange, the maximum tensile stress thereat is also reduced. It should be noted that by adopting a 2-lift casting schedule, though the maximum temperature is reduced to lower than 70ºC, the thermal gradient is as high as 30.2ºC/m and the tensile stress is exceeding the tensile strength of concrete at the same age. It is envisaged that further increasing the number of lifts would not bring about major improvements, but would be highly undesirable from practical viewpoint. Therefore, the use of other thermal cracking control measures with or without combining the 2-lift casting schedule is more advisable.

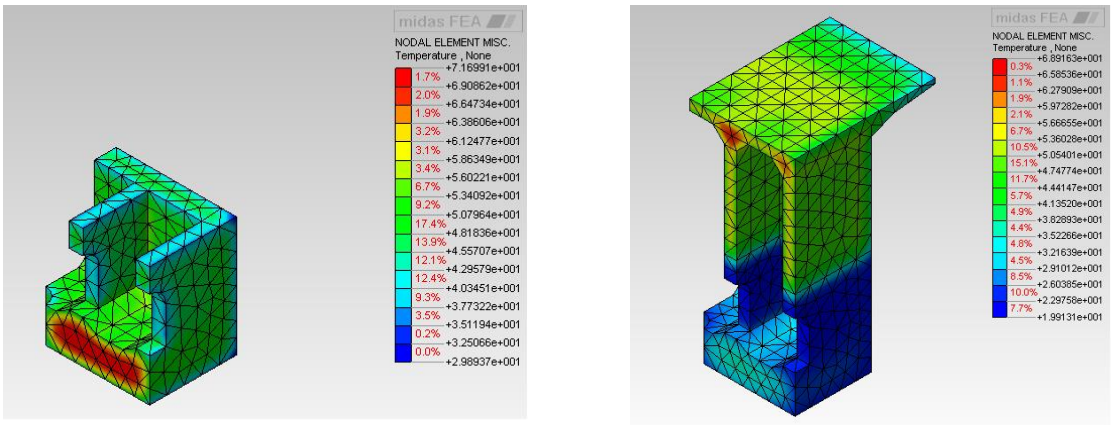

(a) 24 hours after first concrete casting (b) 24 hours after second concrete casting

Figure 8 Computed temperature distributions with casting in lifts

Table 4 Effects of casting in lifts

	Casting in single lift			Casting in 2 lifts			Difference		
	(1)	(2)	(3)	(4)	(5)	(6)	(4) – (1)	(5) – (2)	(6) – (3)
Location	Top flange	Web	Bottom flange	Top flange	Web	Bottom flange	Top flange	Web	Bottom flange
Peak temperature (ºC)	52.27	63.25	71.67	52.28	63.31	68.64	0.01	0.06	-3.03
Max. temperature differential (ºC)	6.58	13.72	21.90	6.57	13.69	19.59	-0.01	-0.03	-2.31
Max. tensile stress (MPa)	1.07	1.00	1.71	0.96	0.99	1.62	-0.11	-0.01	-0.09

CONCLUDING REMARKS

The issues of hydration temperature rise and early thermal cracking should be duly considered in mass concrete construction, including mass concrete elements in bridges such as piles, pile caps, bridge piers, crosshead girders, and bridge diaphragms. The early age temperature rise and thermal stresses induced in the typical segment-on-pier accommodating the diaphragm of prestressed concrete box girder deck of Jinghe Bridge in Gansu Province, Mainland China have been investigated, with the aim to control and mitigate the risk of early thermal cracking. The segment-on-pier has been instrumented with embedded sensors for on-site monitoring of temperature rise. Besides, numerical analysis by finite element method has been conducted to evaluate the temperature distributions and thermal stresses induced in the segment-on-pier at different time. It has been found that the peak temperature at the bottom flange and the maximum thermal gradients caused by temperature differentials of the segment would be excessive, and the computed maximum tensile stresses at the bottom flange would exceed the tensile strength of concrete, indicating the vulnerability of the segment to thermal cracking problem. Temperature control measures should be applied during construction to mitigate the risk of thermal cracking. The effectiveness of adopting concrete mixes containing pulverized fuel ash to replace part of the cement as well as casting of concrete in lifts have been evaluated. With reference to the computation results

revealed from the current study, it is recommended to combine different thermal cracking control measures and optimise the mitigation measures with the aid of finite element analysis as demonstrated in this paper.

REFERENCES

ACI Committee 207 (2005). *Guide to Mass Concrete*, *ACI 207.1R-05*, American Concrete Institute, USA, 30pp.

Architectural Services Department (2011). *Particular Specification for Reinforced Massive Concrete Structures*, 2011 Edition, The Government of Hong Kong SAR, Hong Kong.

Bamforth, P.B. (2007). *Early-Age Thermal Crack Control in Concrete*, *CIRIA C660*, Construction Industry Research and Information Association, UK, 112.

Comite Euro-International du Beton (1993). *CEB-FIP Model Code 1990: Model Code for Concrete Structures*, Thomas Telford, UK, 437.

De Schutter, G. (2002). "Finite element simulation of thermal cracking in massive hardening concrete elements using degree of hydration based material laws". *Computers and Structures*, 80(27-30), 2035-2042.

Du, J.S., Luo, X.F., Ng, P.L. and Au, F.T.K. (2011). "Early age temperature rise and thermal stresses induced in concrete bridge pier". *Advanced Materials Research*, 163-167, 2731-2737.

Kwan, A.K.H., Ng, I.Y.T. and Ng, P.L. (2004). "Mitigating early thermal cracking in concrete structures: Restraint analysis, mix design and thermal control". *American Concrete Institute China Chapter Inaugural Symposium - Challenges in Concrete Technology*, Hong Kong, 1-16.

MTRC (2009). *Materials and Workmanship Specification for Civil Engineering Works*, Section 11, MTR Corporation Limited, Hong Kong.

Ng, P.L. and Kwan, A.K.H. (2012). "Semi-adiabatic curing test with heat loss compensation for evaluation of adiabatic temperature rise of concrete". *HKIE Transactions*, The Hong Kong Institution of Engineers, 19(4), 11-19.

Ng, P.L., Ng, I.Y.T., Fung, W.W.S., Chen, J.J. and Kwan, A.K.H. (2011). "Adiabatic temperature rise of pulverized fuel ash (PFA) concrete". *Advanced Materials Research*, 168-170, 570-577.

Springenschmid, R. (1995). *Thermal Cracking in Concrete at Early Ages*, Proceedings of the International RILEM Symposium, Munich, Germany, E&FN Spon, London, UK, 470.

Zhu, B.F. (1998). *Thermal Stresses and Temperature Control of Mass Concrete*, China Electricity and Power Press, China, 738pp (in Chinese).